Comparison of Sensitive Volumes Associated With Ion- and Laser-Induced Charge Collection in an Epitaxial Silicon Diode

Kaitlyn L. Ryder, *Student Member, IEEE*, Landen D. Ryder, *Student Member, IEEE*, Andrew L. Sternberg, *Member, IEEE*, John A. Kozub, En Xia Zhang, *Senior Member, IEEE*, Ani Khachatrian, *Member, IEEE*, Steven P. Buchner, Dale P. McMorrow, *Fellow, IEEE*, Joel M. Hales, *Member, IEEE*, Yuanfu Zhao, Liang Wang, Chuanmin Wang, Robert A. Weller, *Senior Member, IEEE*, Ronald D. Schrimpf, *Fellow, IEEE*, Sharon M. Weiss, *Senior Member, IEEE*, and Robert A. Reed, *Fellow, IEEE*

***Abstract*—A sensitive volume is developed using pulsed laser-induced collected charge for two bias conditions in an epitaxial silicon diode. These sensitive volumes show good agreement with the experimental two-photon absorption laser-induced collected charge at a variety of focal positions and pulse energies. When compared to ion-induced collected charge, the laser-based sensitive volume overpredicts the experimental collected charge at low bias and agrees at high bias. A sensitive volume based on ion-induced collected charge adequately describes the ion experimental results at both biases. Differences in the amount of potential modulation explain the differences between the ion- and laser-based sensitive volumes at the lower bias. Truncation of potential modulation by the highly doped substrate, at the higher bias, results in similar sensitive volumes.**

***Index Terms*—Pulsed laser, sensitive volume, single-event effects, single-event transients (SETs), two-photon absorption (TPA).**

I. Introduction

THE single-event-effects (SEE) sensitive volume model was first defined in [1] in order to relate the energy deposited in a sensitive volume by an ionizing radiation event to a circuit response. In order to enable the on-orbit estimation of single-event-effects rates, various versions of the sensitive volume model have been developed and used successfully. Early versions of the sensitive volume model defined the sensitive volume geometry as a rectangular parallelepiped (RPP) [1], [2]. Recent methods define a more complex sensitive volume geometry [3], [4] utilizing nested RPPs with varying collection efficiencies. Experimentally determined sensitive volumes typically found at ground-based ion testing facilities are often used as inputs to error rate calculation simulators, such as the CRÈME96 tool [5]–[7] and the Monte Carlo Radiative Energy Deposition (MRED) [3], [4].

Two-photon absorption (TPA)-based pulsed laser SEE testing is useful because of the refined spatial and temporal control of charge generation within devices while offering increased availability and affordability compared to traditional ion beams [8], [9]. Recent research provides a theoretical and computational framework for quantitatively predicting pulsed laser SEE results [10], [11], empirical correlation of laser and ion results [12], [13], and a laser equivalent linear energy transfer (LET) approach to correlate charge generated from pulsed lasers and ions [14]. These approaches all aim at correlating ion experimental results to laser experimental results. However, it would be useful to develop a quantitative, predictive relationship between ion- and pulsed laser-induced SEEs without first empirically correlating laser and ion responses. A key enabling metric toward this goal is to determine if there is a common geometry for the sensitive volume generally useful for both ion- and laser-induced charge collection estimates.

In this work, a large area Si diode fabricated on an epilayer, similar to that used in [15], is used to compare sensitive volume geometries defined by measurements of ion- and TPA pulsed laser-induced collected charge. A common RPP sensitive volume thickness is determined from laser-induced collected charge measurements combined with optical simulations of laser-induced charge distribution profiles at different pulse energies and bias conditions. This sensitive volume geometry is combined with ion LET curves to predict collected charge from heavy-ion experiments and compared to a sensitive volume defined from ion-induced collected charge. Despite the

Manuscript received July 5, 2019; revised September 13, 2019; accepted September 18, 2019. Date of publication September 24, 2019; date of current version January 29, 2020. This work was supported in part by the Defense Threat Reduction Agency through the Basic Research Program under Grant HDTRA1-16-1-0007 and in part by the Sandia National Laboratories LDRD Program.

K. L. Ryder, L. D. Ryder, A. L. Sternberg, E. X. Zhang, R. A. Weller, R. D. Schrimpf, S. M. Weiss, and R. A. Reed are with the Department of Electrical Engineering and Computer Science, Vanderbilt University, Nashville, TN 37235 USA (e-mail: kaitlyn.h.ryder@vanderbilt.edu).

J. A. Kozub is with the Department of Physics and Astronomy, Vanderbilt University, Nashville, TN 37235 USA (e-mail: john.kozub@vanderbilt.edu).

A. Khachatrian, S. P. Buchner, and D. P. McMorrow are with the U.S. Naval Research Laboratory, Washington, DC 37235 USA (e-mail: dale.mcmorrow@nrl.navy.mil).

J. M. Hales is with KeyW Corporation, Herndon, VA 20171 USA (e-mail: joelmh@hotmail.com).

Y. Zhao, L. Wang, and C. Wang are with the Beijing Microelectronics Technology Institute, Beijing 100076, China (e-mail: wangliang150200@163.com).

Color versions of one or more of the figures in this article are available online at http://ieeexplore.ieee.org.

Digital Object Identifier 10.1109/TNS.2019.2943472

0018-9499 © 2019 IEEE. Personal use is permitted, but republication/redistribution requires IEEE permission.
See https://www.ieee.org/publications/rights/index.html for more information.

Authorized licensed use limited to: Vanderbilt University Libraries. Downloaded on July 27,2020 at 15:34:53 UTC from IEEE Xplore. Restrictions apply.

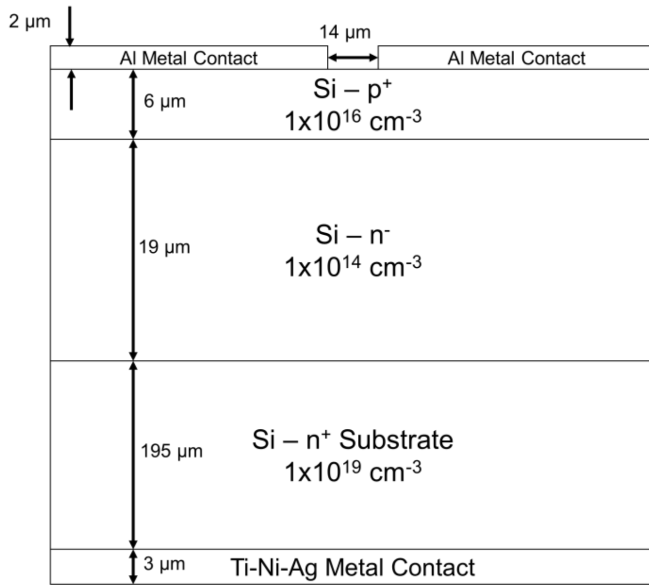

Fig. 1. Cross section of BMTI epitaxial silicon diode. The diode is 2.25 mm^2 and 220-μm thick. The p-n junction occurs roughly 6 μm into the silicon, the epilayer is approximately 19-μm thick, and the substrate starts approximately 25 μm into the silicon. There are 154 μm^2 holes in the top metal contact, allowing for topside illumination.

laser-defined sensitive volume exhibiting good agreement with a laser-induced collected charge under a variety of conditions, it only shows agreement with an ion-induced collected charge under particular bias conditions. The physical mechanisms responsible for the differences are discussed, and limitations of quantitative ion-laser SEE measurements are considered.

II. Experimental Setup

An epitaxial Si diode manufactured by Beijing Microelectronics Technology Institute (BMTI) was used as a test structure in this article. A cross section of the diode is shown in Fig. 1. The devices were manufactured with 154 μm^2 holes in the top Al metal contact, allowing for top-side illumination of the junction. The area of the metal holes accounts for less than 0.1% of the total area of the top contact, so electrical performance is not affected by the presence of the holes. The holes in the metallization are small enough to perturb the laser profile via beam attenuation and diffraction when the laser is focused far from the surface of the device. Effects resulting from the optical perturbations and surface reflections on the silicon are accounted for in the optical simulations when estimating the charge generated by the laser pulse.

A detailed description of the measurement setup is found in [16] and [17]. Ion testing was performed at Lawrence Berkeley National Laboratory's (LBNL) 88" Cyclotron using the 10-MeV/u cocktail. The list of ions used is shown in Table I [18]. For all ions, the flux was approximately 10^7 particles$\cdot$cm$^{-2}\cdot$s^{-1}. The diode was biased at -5 and -90 V for all experiments, resulting in depletion region widths of roughly 4 and 15 μm, respectively. A stainless steel pinhole 200 μm in diameter and 100-μm thick was used to isolate ion events to a small area of the active region of the diode, eliminating charge collection produced by ion events outside of the active diode region.

TABLE I
LBNL Ions

Ion	Energy (MeV)	Surface Incident LET (MeV-cm²/mg)	Range in Si (μm)
Xe	1230	59	90.0
Cu	660	21	108
Si	290	6	142

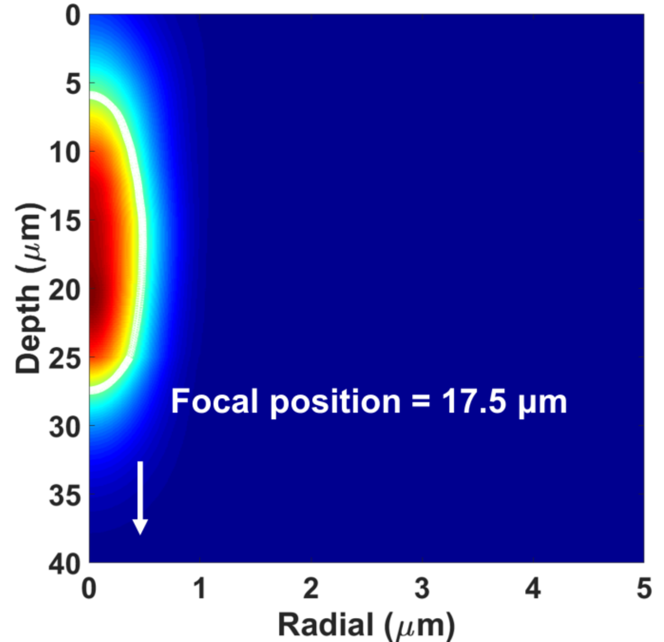

Fig. 2. Normalized time-integrated charge distribution output from Lumerical for a pulse energy of 990 pJ, at a focal position of 17.5 μm. The white arrow shows the direction of pulse propagation and the white contour line shows the FWHM contour of generated charge.

Pulsed laser testing was performed at the Naval Research Laboratory (NRL) Ultrafast Laser Facility [18] using TPA at a wavelength of 1260 nm, and pulse energies of 450, 750, and 990 pJ. The pulse energy was measured using a calibrated linear photodiode [19]. The full-width at half-maximum (FWHM) spot size and temporal width of the laser pulse were 1.36 μm and 130 fs, respectively. A series of measurements made by changing the depth of the laser focus within a device, called a depth scan, was performed.

3-D optical simulations of the laser-induced charge generation profiles were performed using Lumerical, a finite difference time domain (FDTD) nanophotonic simulation software package [20] (described in more detail later). Fig. 2 shows a cross-sectional cut of the simulated time-integrated charge distribution profile from Lumerical using the NRL laser specifications and assuming pulse energy of 990 pJ and a focal position of 17.5 μm. A focal position of 0 μm corresponds to the laser light being focused on the surface of the silicon, and positive focal positions correspond to the laser being focused within the silicon.

Authorized licensed use limited to: Vanderbilt University Libraries. Downloaded on July 27,2020 at 15:34:53 UTC from IEEE Xplore. Restrictions apply.

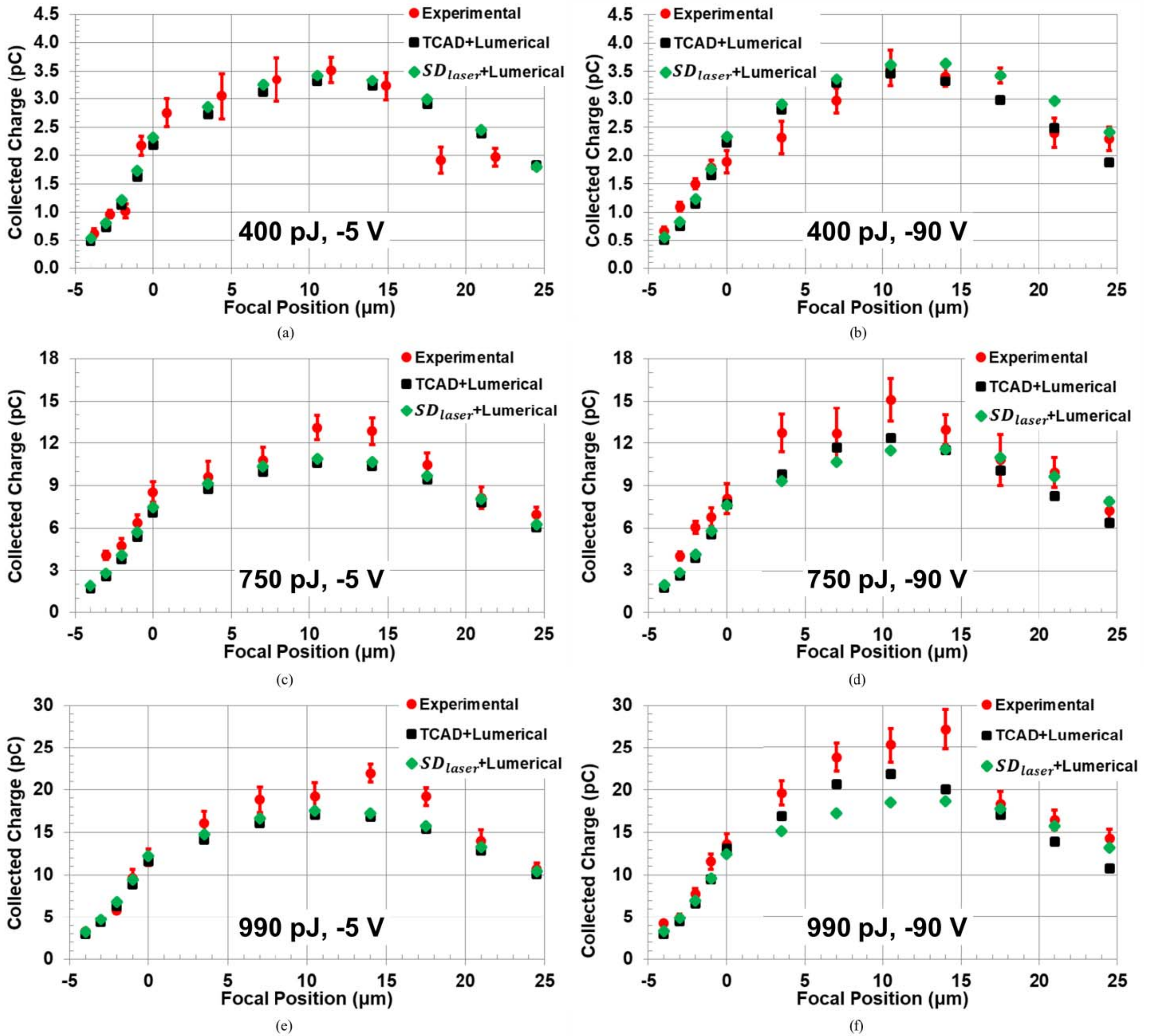

Fig. 3. Collected charge results for a pulse energy of 400 pJ and a bias of (a) −5 V and (b) −90 V, a pulse energy of 750 pJ and a bias of (c) −5 V and (d) −90 V, and a pulse energy of 990 pJ, and a bias of (e) −5 V and (f) −90 V. Experimental results are shown as red circles; the error bars represent one standard deviation given 200 SETs. Lumerical integrated TCAD results are shown as black squares and laser-based sensitive volume predictions are shown as green diamonds. Both the TCAD and sensitive volume predictions show good agreement with the experimental results across all three pulse energies and two biases.

III. Laser-Induced Collected Charge Results

Lumerical FDTD Solutions is a nanophotonic simulation tool that captures optical and nanophotonic effects through a 3-D solution of Maxwell's Equations. Using an approach similar to that reported in [9], Lumerical was modified to account for the following nonlinear effects: Kerr effect, free-carrier refraction and absorption, and TPA [21]. The output from Lumerical is a time-integrated charge distribution, such as that given in Fig. 2. For each pulse energy and focal position in an experiment, a Lumerical charge distribution was generated and ported into Sentaurus TCAD for charge transport simulations. Comparisons between the experimental collected charge and results from the Lumerical—TCAD simulations are given in Fig. 3 (red circles and black squares, respectively) and show good agreement. This suggests that the Lumerical-generated charge distributions are good representations of the physical experiment. Continued investigations into the details of the TCAD simulations, including choice of models and parameters, as well as considerations of possible sources of experimental error, are underway to help improve the accuracy of future work.

A sensitive volume was defined based on the experimental collected charge from laser-induced single-event transients (SETs) and time-integrated charge density profiles from Lumerical. This laser-based sensitive volume was developed

Authorized licensed use limited to: Vanderbilt University Libraries. Downloaded on July 27,2020 at 15:34:53 UTC from IEEE Xplore. Restrictions apply.

assuming: 1) a single sensitive volume with 100% collection efficiency, 2) the volume is radially symmetric and spans the entire device area, and 3) charge collection starts at the surface of the device. These assumptions were informed by TCAD simulations and device layout. Equation (1) is the mathematical expression for the charge collected in the sensitive volume defined here, where $\mathrm{SD_{laser}}$ is the sensitive volume depth of interest, Q_{coll} is the collected charge, $Q_{\mathrm{gen}}(V)$ is the charge generated, V is volume, and A is the surface area. Due to the large scale nature and cylindrical symmetry of this device, the area component of the sensitive volume is the entire device area; for nonsymmetric and highly scaled devices, the particular geometry of the device should be taken into account.

$$Q_{\mathrm{coll}} = \iiint_{V=A\mathrm{SD_{laser}}} \frac{dQ_{\mathrm{gen}}(V)}{dV} dV. \tag{1}$$

A sensitive volume for each bias condition was found using (1) with the experimental collected charge and Lumerical charge distributions from the 24-μm depth position at 990 pJ. This data set was chosen because it represents the most extreme of the possible conditions: 24-μm depth has the most deeply penetrating charge distribution, and pulse energy of 990 pJ is the most likely to show nonlinear effects beyond TPA. Sensitive volume depths of 23 and 26 μm were found for −5 and −90 V, respectively. The collected charge for each of the other experimental focal positions was predicted by integrating their Lumerical charge distributions over the sensitive volumes found, also shown in Fig. 3 (green diamonds). Overall, there is an excellent agreement between experimental, Lumerical-integrated TCAD, and sensitive volume predicted collected charges across all three pulse energies and both biases. Differences between results seen at the higher pulse energy, near the peak of the collected charge, are attributed to the fidelity of the TCAD model and experimental uncertainty. This demonstrates that it is possible to define a single sensitive volume for this diode that well characterizes collected charge for a variety of charge distributions and pulse energies.

IV. Ion-Induced Collected Charge Results

A sensitive volume based on an ion-induced collected charge was determined using a similar method to the laser-based sensitive volume by integrating ion LET curves from the stopping range of ions in matter (SRIM) [22] to find the path length necessary to get the experimental collected charge. This is expressed mathematically in (2), in which $\mathrm{SD_{ion}}$ is the sensitive volume depth of interest, Q_{coll} is the collected charge, $\mathrm{LET}(x)$ is the ion energy loss as a function of depth, ρ is material density (2320 mg/cm^3 for Si), E_{ehp} is the electron-hole pair creation energy (3.6 eV/ehp in Si), and q is the elementary charge

$$Q_{\mathrm{coll}} = \frac{q\rho}{E_{ehp}} \int_0^{\mathrm{SD_{ion}}} \mathrm{LET}(x) dx. \tag{2}$$

An ion-based sensitive volume for each bias condition was determined by finding a sensitive volume for each ion and then taking the average of the three sensitive volumes to get a single volume for each bias. The average was used to account for possible beam contamination and noise in the measurements. Sensitive volume depths of 15 and 25 μm were found for −5 and −90 V biases, respectively.

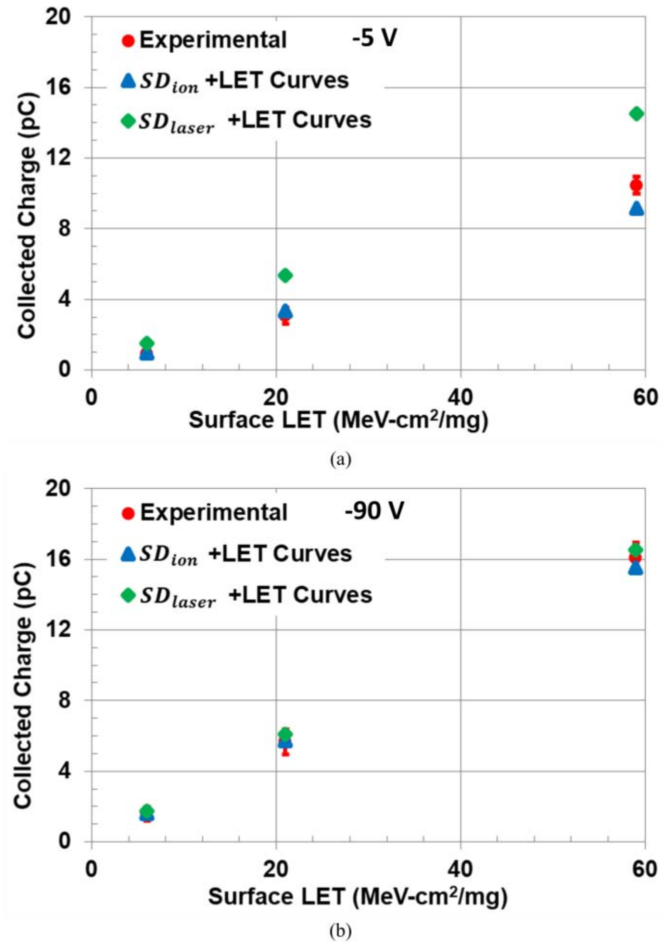

Fig. 4. Ion-induced collected charge results for (a) −5 V bias and (b) −90 V bias. Experimental results are shown as red circles; the error bars represent one standard deviation given 10 000 SETs. Laser-based sensitive volume predictions are shown as green diamonds, and ion-based sensitive volumes are shown as blue triangles. The ion-based sensitive volume predictions show good agreement with the experimental results at both biases, while the laser-based sensitive volume differs from the experimental results at −5 V and agrees at -90 V.

Both the ion- and laser-based sensitive volumes were used to find predicted collected charge for each of the ions by integrating the LET curves over the bias-appropriate sensitive volumes. Fig. 4 shows the ion- and laser-based sensitive volume predictions compared to the experimental results (blue triangles, green diamonds, and red circles, respectively). The ion-based sensitive volume shows reasonable agreement with the experimental results, within 12% for both biases. The laser-based sensitive volume, however, over predicts the collected charge at −5 V by between 40%–75%. There is good agreement between the laser-based sensitive volume prediction and the experimental results at −90 V.

V. Comparison of Sensitive Volumes

A visual comparison of the ion- and laser-based sensitive volumes and the depletion width at the two biases is shown

Authorized licensed use limited to: Vanderbilt University Libraries. Downloaded on July 27,2020 at 15:34:53 UTC from IEEE Xplore. Restrictions apply.

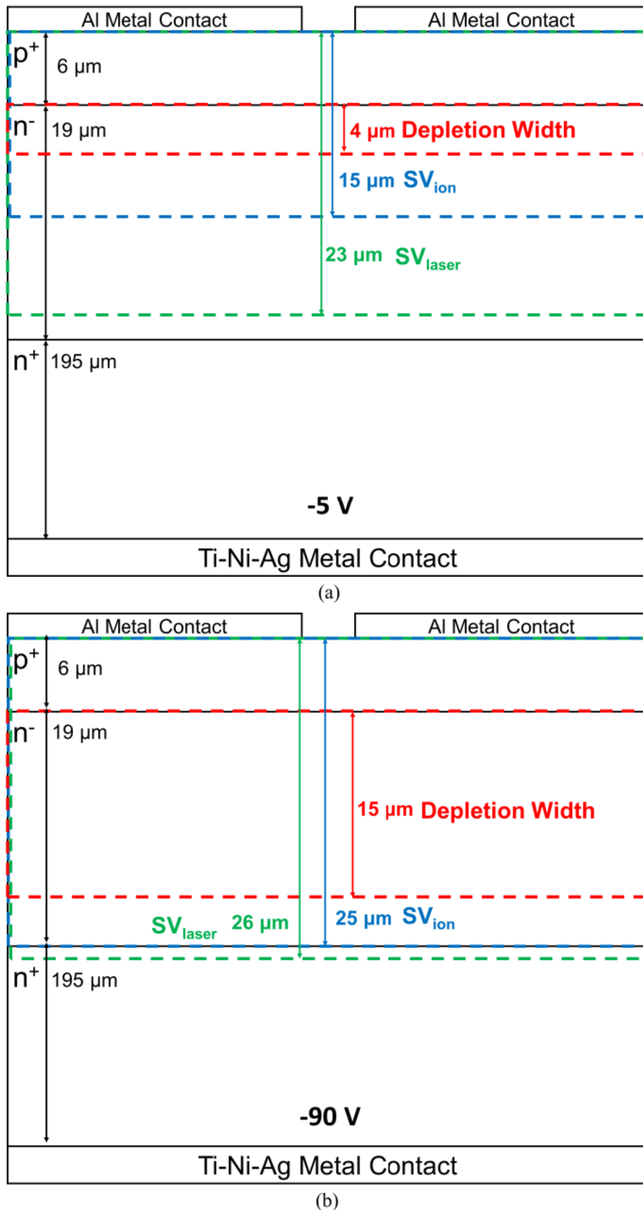

Fig. 5. Comparison for the ion- and laser-based sensitive volumes with the depletion width at (a) −5 V and (b) −90 V. At −5 V, the diode is only slightly depleted and so there is 15 μm of epilayer for potential modulation to occur. At −90 V, the diode is almost fully depleted and potential modulation will be truncated by the substrate after only 4 μm. The sensitive volumes differ when potential modulation is not truncated by the substrate.

in Fig. 5. The depletion width was found mathematically using the depletion approximation and then verified using TCAD. At -5 V, the device is barely depleted with about 15 μm in the epilayer for potential modulation to occur before interactions with the heavily doped substrate occur. It is at this condition that the ion- and laser-based sensitive volumes differ the most, with an 8 μm difference. The sensitive volumes at −90 V are nearly identical when the device is almost fully depleted with only 4 μm of epilayer in which potential modulation can occur. This suggests that the differences in sensitive volume seen at −5 V are due to differences in potential modulation between the ion and laser that get truncated by the substrate when the device is more fully depleted.

Finally, the ion- and laser-based sensitive volumes for both bias conditions were input to CRÈME96 and error rates were found. The error rates used the International Space Station (ISS) orbit with solar minimum and quiet magnetosphere conditions (current solar conditions), and a critical charge of 0.5 pC (minimum collected charge experimentally observed). This resulted in error rates of 2.3×10^{-4} SEEs·s^{-1} (−5 V, ion), 5.3×10^{-4} SEEs·s^{-1} (−5 V, laser), 6.3×10^{-4} SEEs·s^{-1} (−90 V, ion), and 6.8×10^{-4} SEEs·s^{-1} (−90 V, laser). At the lower bias condition, there is more than a factor of two difference in the error rates, whereas there is a negligible difference between the error rates at the higher bias condition. This demonstrates that simply assuming the laser always results in a worse response than that produced by ions is not sufficiently predictive.

VI. Conclusion

Ion- and pulsed laser-induced collected charge experiments were used to define sensitive volumes for an epilayer silicon diode at two bias conditions. The single laser-based sensitive volume describes the collected charge results from the laser experiments at multiple pulse energies and focal positions, whereas the laser-based sensitive volume agrees with ion experimental results only at biases when the device is fully depleted. When the device is not fully depleted, differences in potential modulation between the ion- and laser-induced charge cause the respective sensitive volumes to differ.

The differences in the sensitive volumes describing the ion- and laser-induced collected charges have implications for error rate calculations, one of the main uses for sensitive volumes. The ion- and laser-based sensitive volumes from −5 V were input to CRÈME96, and the laser-based sensitive volume results in an error rate that is over twice as large as the ion-based sensitive volume. By using the laser-based sensitive volume to predict ion-induced SEEs at -5 V results in an overprediction of collected charge and error rate, while at −90 V, the predictions agree with the experimental results.

Despite the differences in the ion- and laser-based sensitive volumes found here, a path forward for using pulsed laser-induced SEEs to predict heavy ion-induced SEEs is still possible. The type of analysis presented here, based on detailed electrical and optical simulations, provides a possible path toward a definition of physically informed sensitive volumes. Using the appropriate simulation tools for each of the charge deposition methods, an understanding of the particular physics that defines the sensitive volumes can be determined. By understanding the differences between the important physics for ion- and laser-induced SEEs, the sensitive volume model for one can be adjusted appropriately to the other. This is correlating simulation spaces and then using the appropriate simulation to predict SEEs, rather than trying to directly correlate experimental ion- and laser-induced SEEs. This process would be particularly useful for highly scaled devices. Light interacts with highly scaled devices and devices with metal-dielectric interfaces much differently than ions [23], which necessitate a greater understanding of the basic physics at play for both ion- and laser-induced SEEs.

Authorized licensed use limited to: Vanderbilt University Libraries. Downloaded on July 27,2020 at 15:34:53 UTC from IEEE Xplore. Restrictions apply.

ACKNOWLEDGMENT

Sandia National Laboratories is a multimission laboratory managed and operated by National Technology and Engineering Solutions of Sandia, LLC., a wholly-owned subsidiary of Honeywell International, Inc., for the U.S. Department of Energy's National Nuclear Security Administration under contract DE-NA-0003525. This article describes objective technical results and analysis. Any subjective views or opinions that might be expressed in the article do not necessarily represent the views of the U.S. Department of Energy or the United States Government.

REFERENCES

[1] L. L. Sivo, J. C. Peden, M. Brettschneider, W. Price, and P. Pentecost, "Cosmic ray-induced soft errors in static MOS memory cells," *IEEE Trans. Nucl. Sci.*, vol. NS-26, no. 6, pp. 5041–5047, Dec. 1979.

[2] E. L. Petersen, "Predictions and observations of SEU rates in space," *IEEE Trans. Nucl. Sci.*, vol. 44, no. 6, pp. 2174–2187, Dec. 1997.

[3] B. D. Sierawski *et al.*, "Impact of low-energy proton induced upsets on test methods and rate predictions," *IEEE Trans. Nucl. Sci.*, vol. 56, no. 6, pp. 3085–3092, Dec. 2009.

[4] K. M. Warren *et al.*, "Application of RADSAFE to model the single event upset response of a 0.25 μm CMOS SRAM," *IEEE Trans. Nucl. Sci.*, vol. 54, no. 4, pp. 898–903, Aug. 2007.

[5] A. J. Tylka *et al.*, "CREME96: A revision of the cosmic ray effects on micro-electronics code," *IEEE Trans. Nucl. Sci.*, vol. 44, no. 6, pp. 2150–2160, Dec. 1997.

[6] M. H. Mendenhall and R. A. Weller, "A probability-conserving cross-section biasing mechanism for variance reduction in Monte Carlo particle transport calculations," *Nucl. Instrum. Methods Phys. Res. A, Accel., Spectrometers, Detectors Associated Equip.*, vol. 667, pp. 38–43, Mar. 2012. doi: 10.1016/j.nima.2.

[7] R. A. Weller *et al.*, "Monte Carlo simulation of single event effects," *IEEE Trans. Nucl. Sci.*, vol. 57, no. 4, pp. 1726–1746, Aug. 2010.

[8] D. McMorrow *et al.*, "Three-dimensional mapping of single-event effects using two photon absorption," *IEEE Trans. Nucl. Sci.*, vol. 50, no. 6, pp. 2199–2207, Dec. 2003.

[9] S. P. Buchner, F. Miller, V. Pouget, and D. P. McMorrow, "Pulsed-laser testing for single-event effects investigations," *IEEE Trans. Nucl. Sci.*, vol. 60, no. 3, pp. 1852–1875, Jun. 2013.

[10] J. M. Hales, A. Khachatrian, N. J.-H. Roche, J. H. Warner, S. P. Buchner, and D. McMorrow, "Simulation of laser-based two-photon absorption induced charge carrier generation in silicon," *IEEE Trans. Nucl. Sci.*, vol. 62, no. 4, pp. 1550–1557, Aug. 2015.

[11] J. M. Hales *et al.*, "Strong correlation between experiment and simulation for two-photon absorption induced carrier generation," *IEEE Trans. Nucl. Sci.*, vol. 64, no. 5, pp. 1133–1136, May 2017.

[12] Z. E. Fleetwood *et al.*, "Using TCAD modeling to compare heavy-ion and laser-induced single event transients in SiGe HBTs," *IEEE Trans. Nucl. Sci.*, vol. 64, no. 1, pp. 398–405, Jan. 2017.

[13] A. Ildefonso *et al.*, "Optimizing optical parameters to facilitate correlation of laser- and heavy-ion-induced single-event transients in SiGe HBTs," *IEEE Trans. Nucl. Sci.*, vol. 66, no. 1, pp. 359–367, Jan. 2019.

[14] J. M. Hales *et al.*, "Experimental validation of an equivalent LET approach for correlating heavy-ion and laser-induced charge deposition," *IEEE Trans. Nucl. Sci.*, vol. 65, no. 8, pp. 1724–1733, Aug. 2018.

[15] S. Buchner *et al.*, "Comparison of single event transients generated at four pulsed-laser test facilities-NRL, IMS, EADS, JPL," *IEEE Trans. Nucl. Sci.*, vol. 59, no. 4, pp. 988–998, Aug. 2012.

[16] I. K. Samsel *et al.*, "Charge collection mechanisms in AlGaN/GaN MOS high electron mobility transistors," *IEEE Trans. Nucl. Sci.*, vol. 60, no. 6, pp. 4439–4445, Dec. 2013.

[17] J. A. Pellish *et al.*, "Heavy ion microbeam- and broadbeam-induced transients in SiGe HBTs," *IEEE Trans. Nucl. Sci.*, vol. 56, no. 6, pp. 3078–3084, Dec. 2009.

[18] M. B. Johnson. *Cocktails and Ions*. Accessed: Jul. 2019. [Online]. Available: http://cyclotron.lbl.gov/

[19] A. Khachatrian, N. J.-H. Roche, D. McMorrow, J. H. Warner, S. P. Buchner, and J. S. Melinger, "A dosimetry methodology for two-photon absorption induced single-event effects measurements," *IEEE Trans. Nucl. Sci.*, vol. 61, no. 6, pp. 3416–3423, Dec. 2014.

[20] Lumerical. *FDTD Solutions*. Accessed: Apr. 2017. [Online]. Available: https://www.lumerical.com/tcad-products/fdtd/

[21] L. D. Ryder, "Simulation of optical energy deposition for pulsed laser-induced single event effects testing in microelectronic devices," M.S. thesis, Dept. Elect. Eng. Comp. Sci., Vanderbilt Univ., Nashville, TN, USA, 2019.

[22] J. F. Ziegler, *SRIM—The Stopping and Range of Ions in Matter*. Accessed: Jul. 2019. [Online]. Available: http://www.srim.org/

[23] L. D. Ryder *et al.*, "Polarization dependence of pulsed laser induced SEEs in SOI FinFETs," *IEEE Trans. Nucl. Sci.*, to be published.

Authorized licensed use limited to: Vanderbilt University Libraries. Downloaded on July 27,2020 at 15:34:53 UTC from IEEE Xplore. Restrictions apply.